A Micromechanical Model for the Fiber Bridging of Macro-Cracks in Composite Plates

G. A. Kardomateas
Associate Professor,
Mem. ASME.

R. L. Carlson
Professor Emeritus.

School of Aerospace Engineering,
Georgia Institute of Technology,
Atlanta, GA 30332-0150

Recent experimental studies on the propagation of transverse cracks in composites have shown that fiber bridging is frequently present, and can be considered as the cause of increased toughness. This paper presents a model that is capable of quantifying this effect and explaining the decrease in the crack growth rate in either a monotonic or a cyclic load profile. Both Modes I and II are considered. The model is based on the elastic loading of a fiber located on the macro-crack face close to the tip and under dominantly plane strain conditions. Two fundamental cases of fiber bridging configurations are distinguished, namely when the fiber-matrix interface is intact and when the fiber-matrix interface has partially failed. Following the single fiber analysis, the model is extended to the case of multiple fibers bridging the faces of the macro-crack. The analysis is for a generally anisotropic material and the fiber lines are at arbitrary angles. Results are presented for the case of an orthotropic material with unidirectional fibers perpendicular to the crack faces. Specifically, the reduction in the stress intensity factor (relative to the nominal value) is investigated for the glass fibers in a glass/epoxy composite system. The effects of fiber debonding and pullout with friction as well as fiber breaking are accounted for in the analysis, and results with respect to a parameter representing the fiber-matrix interface friction are presented. Results are also presented regarding the partial or full fracture of the fiber bridging zone. The model can also be used to analyze the phenomenon of fiber nesting, which is similar to fiber bridging, and occurs with growing delaminations.

Introduction

In many composite structure applications, transverse cracks, usually emanating from holes or notches, extend into sizable macro-cracks growing across the fibers. Fiber bridging of the macro-crack faces has been observed to take place in polymeric matrix composites (e.g., Botsis and Shafiq, 1992) and ceramic-matrix composites (e.g., Zok et al., 1990).

The bridging of macro-cracks by fibers only partially pulled out is a significant source of toughness. The toughening mechanism behind the delamination tip is analogous to the contribution to the toughness of polymers by bridges between molecular chains. Alternatively stated, in plastics, internal stresses are transmitted through tangles of chains, and if crosslinks are present, more and more internal resistance to external loading is available.

The toughening roles played by fibers bridging a crack can be conceptually described as follows: Close to the crack tip, the crack-opening displacement is small enough to be accomodated by enhanced extension of the fiber located there: typical strains to failure are 0.003 for fiberglass and 0.01 for carbon fiber. Moving away from the crack tip, the displacement gets larger so that fiber pull-out or fiber fracture are required in order to accomodate the increasing crack displacement.

This phenomenon has been exploited in the design of various titanium and titanium aluminide alloys which have been reinforced by unidirectional SiC fibers having carbon-rich coatings. These fiber coatings contain weak graphitic films, which facilitate interfacial failure and extensive sliding resisted by friction (e.g. Cox et al., 1989). Such weak interfaces are beneficial in relatively brittle-matrix composites, especially the titanium aluminides, in contrast to the case of the more common ductile metal matrix and polymeric composites, in which stronger interfaces are generally believed to optimize macroscopic properties.

Despite the relatively stronger interfaces of polymetric matrix composites, fiber bridging has been observed as a source of toughening even in these materials. Moreover, another phenomenon, which is analogous to fiber bridging, appears in polymeric matrix composites with growing delaminations. This is the phenomenon of fiber nesting, which takes place because of the fibers which cross adjacent layers due to compression during the manufacturing process (Russell and Street, 1988). As the delamination extends, these nested (bridged) fibers gradually become strained and subsequently divert some of the available strain energy away from the crack tip; therefore increasing the toughness.

The fiber bridging effect on the opening of macro-cracks in composites is analogous to the effect of discrete asperities in the obstruction to crack closure in metallic materials (Beevers et al., 1984; Carlson et al., 1991). However, the fiber bridging of delaminations in composites affects the loading phase (opening of the delamination) and hence it can influence both the monotonic and cyclic growth behavior, whereas the discrete asperities effect in metallic cracks affects the unloading phase (closing of the cracks) and hence this phenomenon influences primarily the cyclic growth behavior. In both cases, the result is a reduced growth rate. In the same context, it can be argued that just as the plastic crushing of discrete asperities can result in an acceleration of fatigue crack growth in metals following a compressive excursion (Kardomateas and Carlson, 1994), the fracture of fiber bridges can similarly result in an acceleration of crack growth in composites following a tensile overload in a cyclic load sequence. Furthermore, it should be noted that fatigue crack growth of metals in an inert atmosphere may,

Contributed by the Applied Mechanics Division of THE AMERICAN SOCIETY OF MECHANICAL ENGINEERS for publication in the ASME JOURNAL OF APPLIED MECHANICS.

Discussion on this paper should be addressed to the Technical Editor, Professor Lewis T. Wheeler, Department of Mechanical Engineering, University of Houston, Houston, TX 77204-4792, and will be accepted until four months after final publication of the paper itself in the ASME JOURNAL OF APPLIED MECHANICS.

Manuscript received by the ASME Applied Mechanics Division, May 16, 1994; final revision, Oct. 18, 1994. Associate Technical Editor: I. M. Daniel.

during unloading, result in a welding of asperities, which would produce an effect similar to the bridging phenomenon discussed here (Carlson and Beevers, 1992).

Several important contributions have appeared on the bridging problem, mainly in connection with ceramic matrix composites. Specifically, Budiansky and Amazigo (1989) examined the effect of fiber bridging on the Mode I stress intensity factor in a smeared fiber force model. Rubinstein and Xu (1992) also examined the effect of fiber bridging on the Mode I stress intensity factor by using a discrete fiber representation in an isotropic material and a linear fiber force-displacement relationship. Nemat-Nasser and Hori (1987) developed asymptotic solutions for fully or partially bridged cracks. A detailed treatment of the fiber debonding with friction was provided by Hutchinson and Jensen (1990).

In the present paper, a different approach is followed, based on discrete fibers at arbitrary orientations, with allowance for fiber breaking. The analysis allows evaluation for both Mode I and II stress intensity factors and is valid for a generally anisotropic material. Also, by incorporating the capability of treating individual fibers, it is possible to examine cases in which single fibers are either fractured or have interface failures which are very different from their adjacent neighbors; such studies would be analogous to examining the effect of imperfections in structural systems. Two cases are treated separately here: either the fiber-matrix interface remains intact or has failed. For the latter case, a general nonlinear fiber force-displacement relationship is proposed.

Formulation

Let us first define the basic geometric and material parameters that will be used in formulating the model. Consider a fiber at an angle ω and at a distance c from the tip of a macro-crack in a composite body of thickness t (Figs. 1(a),(b)). The length of the macro-crack is $2a$ and the fiber is at a distance b from the center. The presence of both externally applied forces and crack face forces is illustrated in Fig. 1(a), whereas the details of the proposed model are indicated in Fig. 1(b). Only the upper crack face is shown with the fiber developing a force with components P and Q.

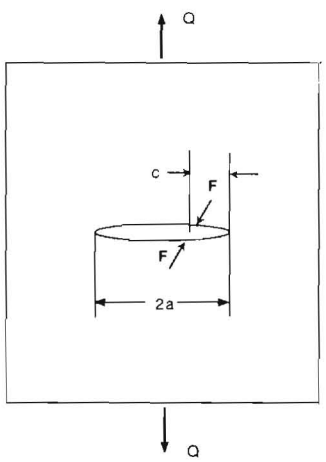

Fig. 1(a) External (global) and crack face (local) loading

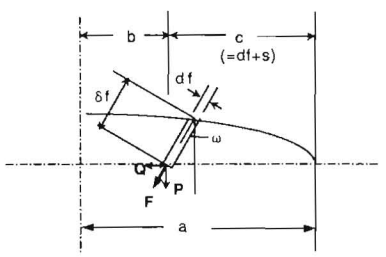

Fig. 1(b) A single fiber loading the upper crack face

Let us consider a state of plane strain, i.e., $\epsilon_{zz} = \gamma_{yz} = \gamma_{xz} = 0$. In this case, the stress-strain relations for the orthotropic body are (Lekhnitskii, 1963):

$$\begin{bmatrix} \epsilon_{xx} \\ \epsilon_{yy} \\ \epsilon_{zz} \\ \gamma_{xy} \end{bmatrix} = \begin{bmatrix} \alpha_{11} & \alpha_{12} & \alpha_{13} & \alpha_{16} \\ \alpha_{12} & \alpha_{22} & \alpha_{23} & \alpha_{26} \\ \alpha_{13} & \alpha_{23} & \alpha_{33} & \alpha_{26} \\ \alpha_{16} & \alpha_{26} & \alpha_{36} & \alpha_{66} \end{bmatrix} \begin{bmatrix} \sigma_{xx} \\ \sigma_{yy} \\ \sigma_{zz} \\ \tau_{xy} \end{bmatrix}, \quad (1)$$

where α_{ij} are the compliance constants (we have used the notation $1 \equiv x$, $2 \equiv y$, $3 \equiv z$).

Using the condition of plane strain, which requires that $\epsilon_{zz} = 0$, allows elimination of σ_{zz}, i.e.,

$$\sigma_{zz} = -\frac{1}{\alpha_{33}}(\alpha_{13}\sigma_{xx} + \alpha_{23}\sigma_{yy}). \quad (2)$$

The Eq. (1) can then be written in the form

$$\begin{bmatrix} \epsilon_{xx} \\ \epsilon_{yy} \\ \gamma_{xy} \end{bmatrix} = \begin{bmatrix} \beta_{11} & \beta_{12} & \beta_{16} \\ \beta_{12} & \beta_{22} & \beta_{26} \\ \beta_{16} & \beta_{26} & \beta_{66} \end{bmatrix} \begin{bmatrix} \sigma_{xx} \\ \sigma_{yy} \\ \tau_{xy} \end{bmatrix}, \quad (3)$$

where

$$\beta_{ij} = \alpha_{ij} - \frac{\alpha_{i3}\alpha_{j3}}{\alpha_{33}} \quad (i, j = 1, 2, 4, 5, 6). \quad (4)$$

Problems of this type can be formulated in terms of two complex analytic functions $\Phi_k(z_k)$ $(k = 1, 2)$ of the complex variables $z_k = x + s_k y$, where s_k, $\bar{s}_k$, $k = 1, 2$ are the roots of the algebraic equation

$$\beta_{11}s^4 - 2\beta_{16}s^3 + (2\beta_{12} + \beta_{66})s^2 - 2\beta_{26}s + \beta_{22} = 0. \quad (5)$$

It was proven by Lekhnitskii (1963) that these roots s_1, s_2, $\bar{s}_1$, $\bar{s}_2$ are either complex or purely imaginary, i.e., Eq. (5) cannot have real roots.

Now we proceed to the problem of studying the effect of discrete loads on a crack face in an anisotropic material.

I Concentrated Equilibrating Forces on the Two Faces of a Macro-Crack in an Anisotropic Material. As has been discussed, following Lekhnitskii (1963), the plane-strain anisotropic elasticity problem can be reduced to that of determining the two complex potentials $\Phi_k(z_k)$ of two different complex variables, $z_k = x + s_k y$, $k = 1, 2$. Notice that if the complex potentials Φ_k are regarded as functions of the complex variables z_k, they must be determined not in the region S but in regions S_k, obtained from S by the affine transformation

$$x_k = x + \alpha_k y, \quad y_k = \beta_k y \quad (k = 1, 2), \quad (6)$$

where $s_k = \alpha_k + i\beta_k$.

For a crack of length $2a$ in the z-plane (Fig. 2), Sih and Liebowitz (1968) have shown that K_I and K_{II} can be evaluated directly from $\Phi_1(z_1)$ in the limit as $z_1 \to a$; i.e.,

$$K_I + \frac{K_{II}}{s_2} = 2\sqrt{2}\left(\frac{s_2 - s_1}{s_2}\right) \lim_{z_1 \to a} \sqrt{z_1 - a}\,\Phi_1'(z_1). \quad (7)$$

In many extensional problems the use of conformal mapping is an efficient method for obtaining the stress intensity factors.

Let the mapping function be defined (with the usual restrictions as to analyticity and single-valuedness) by

$$z = \omega(\zeta); \quad z_k = \omega_k(\zeta_k). \quad (8)$$

Essentially, we map all three regions S, S_1, S_2 onto the $\zeta = \xi + i\eta$ plane (Fig. 2). This mapping is effected so that one and the same point on the contour of the ζ-plane region will corre-

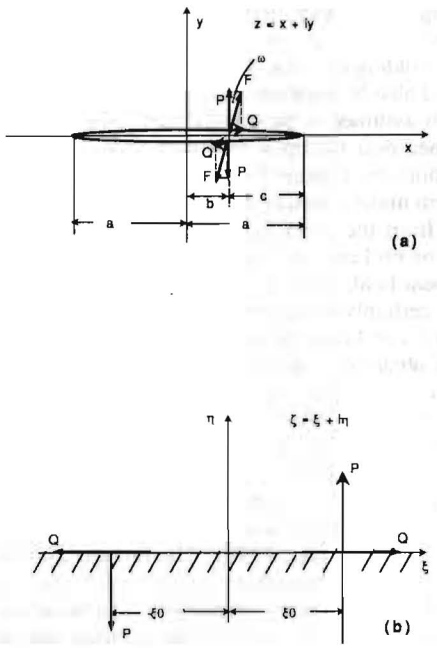

Fig. 2(*a*) The *z*-plane with the crack in an anisotropic body; (*b*) the transformed, ζ-plane

spond to the points on the contours of the regions S and S_k, which are related by the affine transformation (6).

Then

$$\Phi_1'(z_1) = \frac{d\Phi_1}{d\zeta_1}\frac{d\zeta_1}{dz_1} = \frac{\Phi_1'(\zeta_1)}{\omega_1'(\zeta_1)}. \tag{9}$$

Now, corresponding to the crack tip $z = z_1 = a$ in the z-plane, there will be a point $\zeta = \zeta_c$ in the ζ-plane. Thus, Eq. (7) may be written

$$K_I + \frac{K_{II}}{s_2} = 2\sqrt{2}\left(\frac{s_2 - s_1}{s_2}\right)\lim_{\zeta_1 \to \zeta_c}[\omega_1(\zeta_1) - \omega_1(\zeta_c)]^{1/2}\frac{\Phi_1'(\zeta_1)}{\omega_1'(\zeta_1)}. \tag{10}$$

The above equation illustrates the fact that the stress intensity factors may be found simply from a knowledge of $\Phi_1'(z_1)$ in the vicinity of the crack tip, and that Φ_2 can be ignored if the stress intensity factors are the only desired result.

In the $z = x + iy$ plane, we have the region S in the form of an infinite plane with a crack (Fig. 2(*a*)), for which the equation is

$$x = a\cos\theta, \quad -\pi < \theta < \pi; \quad y = 0. \tag{11a}$$

Since $z_k = x + s_k y$, the regions S_1 and S_2 are also planes with straight cutouts described by

$$x_k = x = a\cos\theta, \quad -\pi < \theta < \pi; \quad y_k = y = 0, \quad (k = 1, 2). \tag{11b}$$

As has been already observed, we map all three regions S, S_1, S_2 onto the lower half of the plane $\zeta = \xi + i\eta$. This mapping is effected so that to all three points on the contours of the regions S and S_k corresponds one and the same point on the real axis $\zeta = \xi$.

$$z = \omega(\zeta) = a\left(\frac{1 - \zeta^2}{1 + \zeta^2}\right); \quad z_k = \omega(\zeta_k). \tag{12a}$$

The functions reciprocal to the above, are

$$\zeta = \left(\frac{a - z}{a + z}\right)^{1/2}; \quad \zeta_k = \left(\frac{a - z_k}{a + z_k}\right)^{1/2}. \tag{12b}$$

Indeed, when x and y runs along the contour of the crack, taking on values $x = a\cos\theta$ and $y = 0$, then (12*b*) results in the values

$$\zeta = \zeta_k = \tan(\theta/2) \quad (k = 1, 2). \tag{13}$$

That is, a crack of length $2a$ in the z-plane is transformed to the entire real axis of the ζ-plane, and the infinite plane to the lower half of the ζ-plane. The crack tip $z = a$ is mapped onto the point $\zeta = 0$, and $z = -a$ is mapped onto the two infinite points on the real axis $\zeta = \pm\infty$. Therefore, the upper crack face on the z-plane is mapped onto the positive real semi-axis of the ζ-plane and the lower crack face is mapped onto the negative real semi-axis. Since one point z in the z-plane corresponds to the two points $\pm\zeta$ in the ζ-plane, a one-to-one, conformal transformation is established between the z-plane and the lower half of the ζ-plane.

For a generally anisotropic material, the function $\Phi_1'(\zeta_1)$ for two equilibrating concentrated loads on the half-plane, applied at $\zeta = \pm\zeta_0$, with components P (vertical) and Q (horizontal) is (Lekhnitskii, 1963)

$$\Phi_1'(\zeta_1) = \frac{Ps_2 + Q}{\pi i}\frac{1}{(s_1 - s_2)}\left[\frac{1}{(\zeta_0 - \zeta_1)} - \frac{1}{(-\zeta_0 - \zeta_1)}\right]. \tag{14}$$

Then, upon noting that

$$\lim_{\zeta_1 \to 0}[\omega(\zeta_1) - \omega(0)]^{1/2}\frac{1}{\omega'(\zeta_1)} = -\frac{i\sqrt{2}}{4\sqrt{a}},$$

and that

$$\lim_{\zeta_1 \to 0}\frac{1}{\zeta_0 - \zeta_1} = \frac{1}{\zeta_0} = \left(\frac{a + z_0}{a - z_0}\right)^{1/2},$$

and using (10) and (14), since $z_0 = b$, we obtain for a generally anisotropic body (at the right end of the crack):

$$K_I + \frac{K_{II}}{s_2} = \frac{Ps_2 + Q}{\pi s_2\sqrt{a}}\left(\frac{a + b}{a - b}\right)^{1/2}, \tag{15a}$$

so that the stress intensity factors are given directly as

$$K_I = \frac{P}{\pi\sqrt{a}}\left(\frac{a + b}{a - b}\right)^{1/2}; \quad K_{II} = \frac{Q}{\pi\sqrt{a}}\left(\frac{a + b}{a - b}\right)^{1/2}. \tag{15b}$$

Hence, the relations (15) give the stress intensity factors for an anisotropic infinite sheet with a crack along the x-axis of length $2a$, centered at the origin, and having two equilibrating forces at $x = b$, one on the upper crack face and the other on the lower crack face, with y-component, P, and x-component, Q (per unit thickness).

Notice that since the loads on the crack faces are self-equilibrating, the stress intensity factors do not depend on the material constants. This observation has also been made by Sih et al. (1965); moreover, in analyzing plane center-crack problems, Sih et al. (1965) were able to conclude that "for problems involving self-equilibrating loads (on each boundary) the stress intensity factors for both the isotropic and the anisotropic materials are identical." Only if these loads are not self-equilibrating on each boundary, do the stress intensity factors depend on the elastic constants. A similar statement has been made in connection with the stress distribution in multiply connected bodies by Timoshenko and Goodier (1970). Specifically, they concluded that "the stress

distribution is independent of the elastic constants of the material if the resultant of the forces applied to each boundary are zero. The moment of these forces need not be zero." Notice that this conclusion is of practical importance in the experimental determination of the stress distribution for any material by simply applying the optical methods on a transparent material.

Sih et al. (1965) treated the problem of a single, unbalanced, vertical force, P, on the upper crack face by using a mapping function that transforms the crack in the z-plane into a circular hole of unit radius in the ζ-plane. Since the force was unbalanced, their stress intensity factors included the material constants; however, if an equilibrating force on the lower crack face is included, then their formulas would reduce to the stress intensity factors (15), independent of the elastic constants.

Although the stress intensities are decoupled and independent of the elastic constants, the displacement relationships are not, as will be shown in the next section which considers the development of the fiber-bridging model. The basic configuration of an anisotropic infinite body loaded with remote normal stress σ_0 and in-plane shear τ_0 would also exhibit this feature of decoupled and independent of the elastic constants stress intensities, with $K_I = \sigma_0\sqrt{a}$ and $K_{II} = \tau_0\sqrt{a}$, but the displacements would be coupled (Sih and Chen, 1981).

Hence, it is re-emphasized that since during fiber bridging the loads on the crack faces are self-equilibrating, the stress intensity factors do not depend on the elastic constants for either the isotropic or the anisotropic material assumption.

Next, we shall use these relations in the development of the fiber bridging model.

II Development of the Fiber-Bridging Model. In terms of the stress intensity factors K_I and K_{II}, Sih and Liebowitz (1968) give relations for the displacement field as

$$u_x(r, \theta) = \sqrt{2r}\ \mathrm{Re}\left\{\frac{1}{s_1 - s_2}\left[(K_I s_1 + K_{II})p_2\sqrt{\cos\theta + s_2\sin\theta} - (K_I s_2 + K_{II})p_1\sqrt{\cos\theta + s_1\sin\theta}\right]\right\}, \quad (16a)$$

$$u_y(r, \theta) = \sqrt{2r}\ \mathrm{Re}\left\{\frac{1}{s_1 - s_2}\left[(K_I s_1 + K_{II})q_2\sqrt{\cos\theta + s_2\sin\theta} - (K_I s_2 + K_{II})q_1\sqrt{\cos\theta + s_1\sin\theta}\right]\right\}, \quad (16b)$$

where

$$p_k = \beta_{11}s_k^2 + \beta_{12} - \beta_{16}s_k; \quad q_k = \beta_{12}s_k + \frac{\beta_{22}}{s_k} - \beta_{26}, \ k = 1, 2. \quad (16c)$$

At a distance c behind the crack tip, i.e., at $\theta = \pi$ and $r = c$, the displacements become

$$u_x = \sqrt{2c}\ \mathrm{Im}\left\{\frac{1}{s_2 - s_1}\left[K_I(s_1p_2 - s_2p_1) + K_{II}(p_2 - p_1)\right]\right\}, \quad (17a)$$

$$u_y = \sqrt{2c}\ \mathrm{Im}\left\{\frac{1}{s_2 - s_1}\left[K_I(s_1q_2 - s_2q_1) + K_{II}(q_2 - q_1)\right]\right\}. \quad (17b)$$

The displacements at the lower crack face, i.e., at $\theta = -\pi$, are of opposite sign.

Notice that even if a pure Mode I state of loading exists, i.e., $K_{II} = 0$, both normal and shear components of the displacement field u_y and u_x, respectively, are nonzero for general anistropy. This means that the final orientations of the bridging fibers, ω_i, may be slightly different than the initial fiber orientations. They will be determined in the process of fiber loading, and are, therefore, unknowns to be determined.

It should also be mentioned that the length of the fiber bridging zone is assumed to be small compared to the crack length, and confined near the tip of the crack. Therefore, the displacement relations are expected to be adequate near the crack tip for the problem under consideration. In practical cases, at moderate distances from the crack tip, the fibers would actually be expected to be broken, anyway. A more accurate solution for the displacement field, valid at large distances away from the crack tip would certainly be desirable; however, it is not available at present and our future plans include exploring the theoretical aspects of obtaining a more accurate displacement field for an anisotropic crack. This would then be directly incorporated into our fiber bridging model. Future research could also include detailed finite element analyses. Please note that the same assumptions regarding the displacement field, namely use of the asymptoptic near-tip formula, have been adopted in past work of other researchers, such as the discrete asperities model in metals of Beevers et al. (1984). The discrete asperities model has been applied to the closure obstruction problem, and it has been found that the features of the model can be used to correlate experimental measurements of opening stress intensity factors after tensile overloads (Carlson et al., 1991).

Now, let us represent the Mode I and Mode II contribution of the global, external load by $K_{I,GL}$ and $K_{II,GL}$, respectively. By superposition, the total stress intensity factor is

$$K_{I,II} = K_{I,II,\mathrm{local}} + K_{I,II,GL}. \quad (18)$$

Displacement conditions at the fiber sites are needed to determine the fiber loads. The displacements at the upper macro-crack face, i.e., at $\theta = \pi$ and an arbitrary r, due to both local and global loading, is

$$u_{x,y}(r, \pi) = u_{x,y,GL} + u_{x,y,\mathrm{local}}. \quad (19)$$

Moreover, if $c = a - b$ represents the initial distance of the fiber load point from the crack tip, this distance on the upper crack face is $c - \delta_f \sin\omega$, and the corresponding distance on the lower crack face is $c + \delta_f \sin\omega$, due to the fiber orientation at an angle ω as shown in Fig. 1(*b*). The quantity δ_f represents half of the final fiber interference length and will be discussed in detail in the following. Hence, including the effect of loading both the upper and lower faces of the macro-crack, and using the stress intensity factors for the global and the local load from (15), we can write the x-component of the displacement difference between the upper, $\theta = \pi$, and lower, $\theta = -\pi$, face of the macro-crack at the fiber site, $r = c$, as follows:

$$\begin{aligned} u_x(c, \pi) = {} & 2\sqrt{2c}\ \mathrm{Im}\left\{\frac{1}{s_2 - s_1}\left[K_{I,GL}(s_1p_2 - s_2p_1) + K_{II,GL}(p_2 - p_1)\right]\right\} \\ & + 2\sqrt{2c}\left[\left(\frac{2a - c + \delta_f\sin\omega}{c - \delta_f\sin\omega}\right)^{1/2} + \left(\frac{2a - c - \delta_f\sin\omega}{c + \delta_f\sin\omega}\right)^{1/2}\right] \\ & \times \mathrm{Im}\left\{\frac{1}{s_2 - s_1}\left[\frac{F\cos\omega}{2\pi\sqrt{a}}(s_1p_2 - s_2p_1) + \frac{F\sin\omega}{2\pi\sqrt{a}}(p_2 - p_1)\right]\right\}, \end{aligned} \quad (20a)$$

and the y-component of the displacement spread (opening) as

$$u_y(c, \pi) = 2\sqrt{2c}\ \mathrm{Im}\left\{\frac{1}{s_2 - s_1}\left[K_{I,GL}(s_1 q_2 - s_2 q_1) + K_{II,GL}(q_2 - q_1)\right]\right\} + 2\sqrt{2c}\left[\left(\frac{2a - c + \delta_f \sin\omega}{c - \delta_f \sin\omega}\right)^{1/2} + \left(\frac{2a - c - \delta_f \sin\omega}{c + \delta_f \sin\omega}\right)^{1/2}\right] \times \mathrm{Im}\left\{\frac{1}{s_2 - s_1}\left[\frac{F\cos\omega}{2\pi\sqrt{a}}(s_1 q_2 - s_2 q_1) + \frac{F\sin\omega}{2\pi\sqrt{a}}(q_2 - q_1)\right]\right\}. \quad (20b)$$

Two separate cases of fiber bridging configurations are distinguished now.

(a) Fiber-Matrix Interface Intact. In this case, which is schematically shown in Fig. 3, the displacement at the fiber site is zero. The fiber is elastically stretched with a force F, therefore the fiber stress is

$$\sigma = \frac{4F}{\pi d_f^2}; \quad \sigma < \sigma_{uf}, \quad (21a)$$

where d_f is the fiber diameter. A condition of the fiber stress being below the fiber ultimate strength σ_{uf} is imposed for validity of this model.

The condition of zero displacement at the fiber site gives

$$u_x(c, \pm\pi) = u_y(c, \pm\pi) = 0. \quad (21b)$$

Taking into account (15b), (17), and (18), it is concluded that the foregoing two equations, (21b), are two linear equations in P and Q. Notice that in this case the fiber can sustain both tensile and shear stresses; the force along the fiber axis is $F = P\cos\omega + Q\sin\omega$.

In this case of an intact fiber-matrix interface, we have very effective ligament bridging. However, it is more reasonable, common, and an experimentally supported fact, that the fiber does not remain perfectly bonded to the matrix and fiber debonding occurs to some extent. This case is examined next.

(b) Partial Fiber-Matrix Interface Debonding. In this case, which is schematically shown in Fig. 1(b), the displacement at the fiber site is nonzero. The characterization of frictional sliding of a fiber embedded in a matrix is an issue of intense current interest. To this extent, Hutchinson and Jensen (1990) have developed a model that describes the interactions between components of a unidirectionally reinforced composite which is subject to debonding. The model is designed to include the effects of fiber strength, interface bond strength, and the friction force which can develop if residual compressive stresses act across the interface boundary.

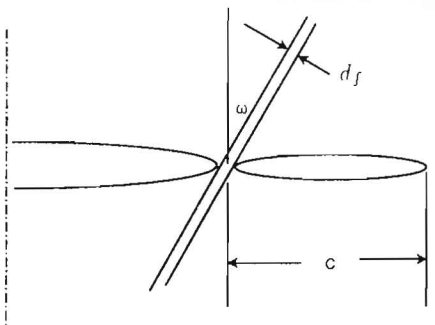

Fig. 3 The case of fiber-matrix interface intact (ligament-bridging)

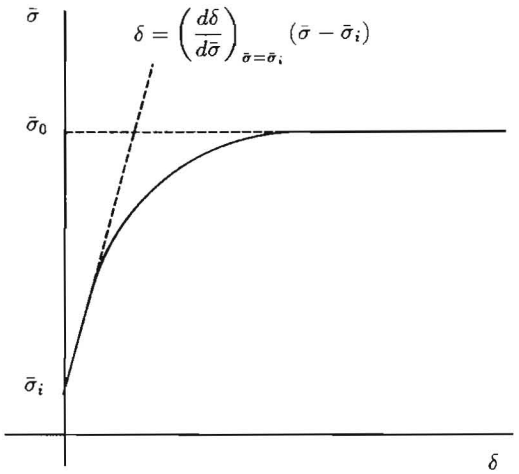

Fig. 4 Schematic of the fiber stress, $\bar{\sigma}$, versus displacement, δ, curve

The form of the fiber stress, $\bar{\sigma}$, versus the pullout displacement, δ, curve with Coulomb friction is qualitatively illustrated in Fig. 4. The fiber stress versus the debond length, l, is similar in form. As shown, the debond length and pullout displacement are zero until a threshold value of stress, $\bar{\sigma}_i$, is achieved. Above this value, the curves have decreasing slopes until a limiting, unstable value of stress, $\bar{\sigma}_0$, is attained. Note that if the fiber strength, $\bar{\sigma}_c$, is less than $\bar{\sigma}_0$, the value of $\bar{\sigma}$ can abruptly decrease and then continuously decrease with increasing δ.

In the following, a_i, b_i, and $\tilde{c}_i$ are constants that depend on the overall modulus of the composite and the elastic properties of the fibers and the matrix, and they are given in the Appendix of Hutchinson and Jensen (1990). An expression for the debond length, l, is given in terms of the coefficient of friction, μ, and the area fraction of the fiber, $\rho = [d_f/(d_f + s)]^2$, as follows

$$l = \frac{d_f}{4\mu b_1} \ln\left[\frac{\bar{\sigma}_0 - \bar{\sigma}_i + k_1(\bar{\sigma}_i - \bar{\sigma})}{\bar{\sigma}_0 - \bar{\sigma}}\right], \quad (22a)$$

where

$$k_1 = \rho(1 - \rho)^{-1} a_3 \tilde{c}_3 / b_1. \quad (22b)$$

When the fiber is isotropic with $\nu_f = \nu_m$, then $a_3 = 0$ and thus $k_1 = 0$.

Moreover, the pullout displacement, δ, is given by Hutchinson and Jensen (1990) in terms of the modulus of the matrix, E_m, and the mode II toughness for the debond crack, measured by the critical value of the energy release rate, G_c:

$$\delta = (b_2 + b_3)\left\{\frac{1 - \rho}{\rho}\frac{l}{\tilde{c}_1 \tilde{c}_3}\left(\frac{2G_c}{E_m d_f}\right)^{1/2} - \frac{d_f \bar{\sigma_r^-}}{4\mu b_1^2 E_m}\left[e^{-\zeta_l} + \zeta_l - 1\right]\right\}, \quad (22c)$$

where $\zeta_1 = 4\mu b_1 l/d_f$ and $\bar{\sigma_r^-}$ is the normal stress acting across the interface just below the debond tip. For debonding with Coulomb friction,

$$\bar{\sigma_r^-} = -\rho^{-1}(1 - \rho)(b_1/\tilde{c}_3)[\bar{\sigma}_0 - \bar{\sigma}_i + k_1(\bar{\sigma}_0 - \bar{\sigma})]. \quad (22d)$$

The previous expressions are nonlinear relations for the fiber displacement versus fiber stress law, $\delta = F(\bar{\sigma})$. Although it

seems that a nonlinear fiber load-displacement relationship would provide a more complete description of the fiber debonding process and better account for the relative sliding between the fiber and the matrix, the need for analytically tracking the problem easily has led to the use of a linear relationship between displacement and fiber load (e.g., Rubinstein and Xu, 1992). It is also easier to illustrate the use of our fiber bridging model by using a linear law.

For this purpose, a linear fiber displacement versus fiber stress law is adopted by using the initial, almost linear segment the curve in Fig. 4, as follows:

$$\delta = \left(\frac{d\delta}{d\bar{\sigma}}\right)_{\bar{\sigma}=\bar{\sigma}_i} (\bar{\sigma} - \bar{\sigma}_i); \quad l = \left(\frac{dl}{d\bar{\sigma}}\right)_{\bar{\sigma}=\bar{\sigma}_i} (\bar{\sigma} - \bar{\sigma}_i). \quad (23a)$$

Such an approximation should be adequate as long as we are not very close to the saturation stress, $\bar{\sigma}_0$.

The resulting expressions are much simpler if we assume that the fiber is isotropic with $\nu_f = \nu_m$ (in which case $k_1 = 0$). Under this assumption, we obtain from (22a, c) and (23a)

$$\delta = (b_2 + b_3)\frac{1-\rho}{\rho\tilde{c}_1\tilde{c}_3}\left(\frac{2G_c}{E_m d_f}\right)^{1/2}\frac{d_f}{4\mu b_1(\bar{\sigma}_0 - \bar{\sigma}_i)}(\bar{\sigma} - \bar{\sigma}_i);$$

$$\text{for } \bar{\sigma}_i < \bar{\sigma} < \bar{\sigma}_0. \quad (23b)$$

The initiation stress $\bar{\sigma}_i$ is the stress required to propagate the debond crack up the fiber and is given in terms of the axial mismatch strain ϵ_z^T by

$$\frac{\bar{\sigma}_i}{E_m\epsilon_z^T} = \frac{1}{\tilde{c}_1}\left(\frac{2G_c}{E_m d_f \epsilon_z^{T2}}\right)^{1/2} - \frac{\tilde{c}_2}{\tilde{c}_1} \quad (23c)$$

In turn, the saturation stress $\bar{\sigma}_0$ is given in terms of the radial mismatch strain ϵ_r^T by

$$\bar{\sigma}_0 = \rho E_f \epsilon_r^T/\nu_f. \quad (23d)$$

The initiation stress can be negative if the nondimensional combination $2G_c/(Ed_f\epsilon_T^2)$ is sufficiently small; in such cases, a finite length debond zone would be introduced before any overall stress is applied. In the interest of simplicity, let us take $\bar{\sigma}_i = 0$ (the case of nonzero $\bar{\sigma}_i$ will be examined in a future publication). Furthermore, since we assume that there is a uniform distribution of fibers with spacing s and diameter d_f through the thickness, there are $1/(d_f + s)$ fibers per unit thickness, and the effective area per unit thickness is $A_f = \pi d_f^2/4(d_f + s)$. Then, (23$b$) gives the fiber displacement $\delta_f = \delta$ in terms of the fiber force $F_i = \bar{\sigma}A_f$, in the form

$$\delta_f = -\tilde{\lambda}\frac{4F_i(d_f + s)}{\pi E_f d_f}, \quad (24a)$$

where now $\tilde{\lambda}$ is dimensionless and can be considered as a measure of the fiber-matrix friction

$$\tilde{\lambda} = (b_2 + b_3)\frac{1-\rho}{\rho\tilde{c}_1\tilde{c}_3}\left(\frac{2G_c}{E_m d_f}\right)^{1/2}\frac{E_f}{4\mu b_1\bar{\sigma}_0}. \quad (24b)$$

The minus sign is used because the fiber is under tension loading when the crack face is loaded with a force opposite to the one in Fig. 2(a); the force in Fig. 2(a) would generate the local stress intensity factors given by (15).

In the previous relations, d_f is the fiber diameter and s is the mean spacing between the fibers. In a representation of the form (24a), the quantity $\tilde{\lambda}$ increases for poorer bond quality that allows more fiber sliding. This quantity can vary widely depending on the class of composites under consideration. Specifically, brittle (ceramic)-matrix composites are characterized by relatively weak interfaces, in contrast to the case of the more common polymeric-matrix composites or the ductile metal-matrix composites, in which relatively strong interfaces generally exist.

Since $2\delta_f$ is the final interference fiber height, the conditions for determining the forces P and Q are the displacements at the fiber site

$$u_x(c, \pi) - u_x(c, -\pi) = 2\delta_f \sin\omega,$$
$$u_y(c, \pi) - u_y(c, -\pi) = 2\delta_f \cos\omega. \quad (25)$$

III Multiple Fiber Bridging. The single fiber analysis has been used thus far because a clear definition of the working quantities was needed. In actual fiber-bridging situations, multiple fibers are connecting the two faces of the macro-crack. Based on the single fiber analysis, an extension to multiple fibers can be directly performed. An interesting observation in connection with the multiple fiber bridging problem is that the load redistribution, which occurs among fiber bridges, as the load increases (or the crack propagates) and some fibers break in the process, is analogous to the redistribution of stresses which occurs due to the development of a crack-tip plastic zone in metallic materials. On another note, it can be observed that a similar redistribution occurs in the shear lag mechanism of load transfer in composites.

If n fibers at final angles ω_i and at distances c_i behind the tip (and b_i from the center) are bridging the faces of the macro-crack, then the first set of conditions for determining the forces P_i and Q_i are the displacement components equations at each of the fiber sites (Fig. 5). A direct extension of Eqs. (20), and using (25), gives the first equation from the x-component of the displacement spread between the upper and lower crack faces as

$$\delta_{fi}\sin\omega_i = \sqrt{2c_i}\,\mathrm{Im}\left\{\frac{1}{s_2 - s_1}[K_{I,GL}(s_1p_2 - s_2p_1) + K_{II,GL}(p_2 - p_1)]\right\}$$
$$+ \sqrt{2c_i}\sum_{j=1}^{n}\left[\left(\frac{2a - c_j + \delta_{fj}\sin\omega_j}{c_j - \delta_{fj}\sin\omega_j}\right)^{1/2} + \left(\frac{2a - c_j - \delta_{fj}\sin\omega_j}{c_j + \delta_{fj}\sin\omega_j}\right)^{1/2}\right]$$
$$\times\,\mathrm{Im}\left\{\frac{1}{s_2 - s_1}\left[\frac{F_j\cos\omega_j}{2\pi\sqrt{a}}(s_1p_2 - s_2p_1) + \frac{F_j\sin\omega_j}{2\pi\sqrt{a}}(p_2 - p_1)\right]\right\}. \quad i = 1, \ldots n \quad (26a)$$

The condition from the y-component of the displacement spread is

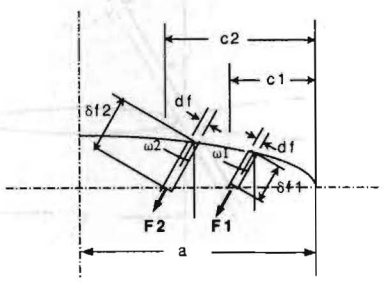

Fig. 5 Loading of multiple fibers on the upper face of the macro-crack

$$\delta_{fi}\cos\omega_i = \sqrt{2c_i}\,\mathrm{Im}\left\{\frac{1}{s_2 - s_1}\left[K_{I,GL}(s_1q_2 - s_2q_1) + K_{II,GL}(q_2 - q_1)\right]\right\}$$

$$+ \sqrt{2c_i}\sum_{j=1}^{n}\left[\left(\frac{2a - c_j + \delta_{fj}\sin\omega_j}{c_j - \delta_{fj}\sin\omega_j}\right)^{1/2} + \left(\frac{2a - c_j - \delta_{fj}\sin\omega_j}{c_j + \delta_{fj}\sin\omega_j}\right)^{1/2}\right]$$

$$\times\,\mathrm{Im}\left\{\frac{1}{s_2 - s_1}\left[\frac{F_j\cos\omega_j}{2\pi\sqrt{a}}(s_1q_2 - s_2q_1) + \frac{F_j\sin\omega_j}{2\pi\sqrt{a}}(q_2 - q_1)\right]\right\}, \quad i = 1, \ldots n. \quad (26b)$$

The second set of conditions is the fiber load-displacement equations, either (22) for a nonlinear law or (23), (24) for a linear law.

The quantities to be determined are the final fiber interference heights δ_{fi} and the fiber loads F_i as well as the fiber orientations ω_i; hence there are $3n$ unknowns. For each fiber there are two displacement equations, (26a, b), and one "fiber constitutive," equation; hence we have a total of $3n$ equations. Therefore, a well-posed problem has been formulated. The only complication arises from the fact that the system of equations is nonlinear.

The problem becomes linear, however, in the more common problem of a transverse crack in a zero-degree unidirectional orthotropic composite under pure Mode I loading, if the linear fiber load-displacement Eq. (24a) is used (Fig. 6). Due to symmetry, $\omega_i = 0$, and the x-displacements are zero and the corresponding relations (26a) are automatically satisfied (because the quantities in the brackets turn out to be real). Furthermore, δ_{fi} can be directly expressed in terms of F_i from the linear fiber load-displacement law. This leaves us with the n fiber loads, F_i, to be determined from the n linear equations from the normal, u_y, displacement relations at the fiber sites, (26b). The number of loaded fibers, n, is determined by imposing the condition of the fiber loads being below the fiber strength, i.e.:

$$-\frac{4F_i(d_f + s)}{\pi d_f^2} < \sigma_{uf}, \quad i = 1, \ldots n. \quad (27)$$

Hence, n is increased successively, until a state is reached where the nth fiber is under load exceeding the fracture strength.

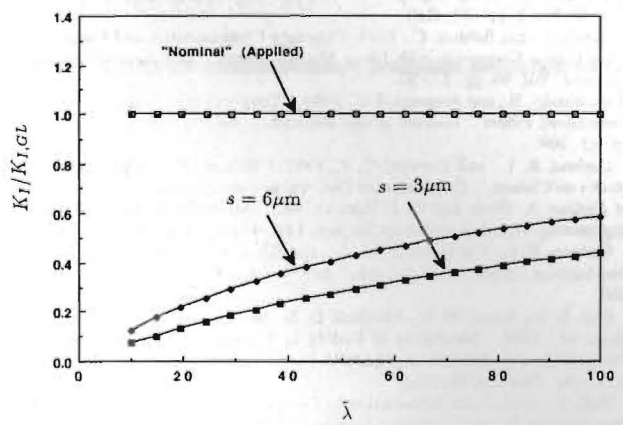

Fig. 6 The "effective" stress intensity factor, K_I, as a function of $\bar{\lambda}$, which expresses the interface friction. Two values of fiber spacing, s, are considered. $K_{I,GL}$ is the nominal (applied) stress intensity factor.

In the general case of an arbitrary fiber orientation, under combined Mode I and II loading with the linear fiber load-displacement relation, again δ_{fi} can be directly expressed in terms of F_i. Furthermore, an initial guess for the final fiber orientations is the initial fiber orientations of the parent composite, ω_i^0. This leaves us with the n fiber loads, F_i, to be determined from the n linear equations for the normal, u_y, displacements at the fiber sites. An iteration procedure can be employed to find the final orientations of the bridging fibers, ω_i, by satisfying the x-displacement equations. Since a neighborhood of the roots is identified, standard numerical techniques such as the Newton-Raphson, generalized to multiple dimensions, can be used (Press et al., 1989).

Once the fiber loads, F_i, and the fiber interference lengths, δ_{fi}, and orientations, ω_i, are determined, the local stress intensity factors can be found by using (15b), as follows:

$$K_{I,\mathrm{local}} = \sum_{j=1}^{n}\frac{F_j\cos\omega_j}{2\pi\sqrt{a}}\left[\left(\frac{2a - c_j + \delta_{fj}\sin\omega_j}{c_j - \delta_{fj}\sin\omega_j}\right)^{1/2} + \left(\frac{2a - c_j - \delta_{fj}\sin\omega_j}{c_j + \delta_{fj}\sin\omega_j}\right)^{1/2}\right], \quad (28a)$$

$$K_{II,\mathrm{local}} = \sum_{j=1}^{n}\frac{F_j\sin\omega_j}{2\pi\sqrt{a}}\left[\left(\frac{2a - c_j + \delta_{fj}\sin\omega_j}{c_j - \delta_{fj}\sin\omega_j}\right)^{1/2} + \left(\frac{2a - c_j - \delta_{fj}\sin\omega_j}{c_j + \delta_{fj}\sin\omega_j}\right)^{1/2}\right]. \quad (28b)$$

Application of the Model

The model described in the previous section has been used to analyze the effect of fiber bridging on a transverse crack in a unidirectional orthotropic plate. The linear fiber load-displacement law, Eq. 24(a), is used. It will be shown that the effect of fiber spacing and the fiber-matrix interface friction can be quantified in this model. Moreover, the response due to increasing magnitudes of tensile loads that may include partial or full fracture of the bridging zone will be investigated.

The composite system considered is a glass/epoxy with glass fibers of diameter $d_f = 11$ μm. Two values of spacing are considered: one with a fiber spacing of $s = 6$ μm and a more closely spaced system, $s = 3$ μm. Notice that the fibers are at distances from the crack tip $c_j = (d_f + s)j$, $j = 1, \ldots n$. For square spacing, this would give fiber volume fractions of $V_f = 0.329$ and $V_f = 0.485$, respectively, according to the formula (e.g., Hull, 1981):

$$V_f = \frac{\pi}{4}\left(\frac{s}{d_f} + 1\right)^{-2}.$$

The glass fibers have a modulus $E_f = 72.5$ GPa and an ultimate strength of $\sigma_{uf} = 3.5$ GPa. The epoxy matrix is assumed to have a shear modulus of $G_m = 1.35$ GPa.

The moduli in GN/m^2 and Poisson's ratios used are listed below, where 1 is the horizontal (x) direction, 2 is the vertical (y), and 3 the direction through the thickness (z).

(a) Spacing of $s = 6$ μm: $E_1 = E_3 = 5.1$, $E_2 = 26.2$, $G_{12} = G_{23} = 2.1$, $G_{31} = 1.9$, $\nu_{12} = 0.068$, $\nu_{23} = 0.277$, $\nu_{31} = 0.400$. The characteristic Eq. (5) gives purely imaginary roots:

$$s_1 = 0.297i; \quad s_2 = 1.609i.$$

Furthermore, Eq. (16c) gives real p_k and purely imaginary q_k.

(b) Spacing of $s = 3$ μm: $E_1 = E_3 = 6.5$, $E_2 = 37$, $G_{12} = G_{23} = 2.6$, $G_{31} = 2.4$, Poisson's ratios are the same as in system (a). For this material, the characteristic Eq. (5) gives again purely imaginary roots:

$$s_1 = 0.277i; \quad s_2 = 1.641i.$$

Furthermore, Eq. (16c) gives again real p_k and purely imaginary q_k.

In either a center-cracked specimen with a crack of length $2a$ or a single-edge crack specimen with a crack of length a under a remotely applied normal stress σ_0, the stress intensity factor is the same as for an isotropic body (e.g., Sih and Chen, 1981):

$$K_{I,GL}(\sigma_0) = \sigma_0\sqrt{a}; \quad K_{II,GL} = 0. \tag{29}$$

A crack length of $a = 10$ mm and a remotely applied stress corresponding to the typical value of fracture toughness of the epoxy matrix are assumed, i.e., $K_{I,GL} = 1.25$ MN/m$^{3/2}$. The remotely applied stress, $\sigma_0 = 12.5$ MPa, and the crack length are also the same as the ones used in the experiments of Botsis and Shafiq (1992) and Botsis and Beldica (1994). Furthermore, a fiber bridging zone of 120 μm behind the crack tip is assumed. For the spacing of $s = 6$ μm, a total of 20 fibers would span this distance, whereas for the spacing of $s = 3$ μm, there would be a total of 40 fibers in the bridging zone.

For the unidirectional case, $\omega = 0$, the local stress intensity factors are given by using (28), as follows:

$$K_{I,\text{local}} = \sum_{j=1}^{n} \frac{F_j}{\pi\sqrt{a}} \left(2 - \frac{c_j}{a}\right)^{1/2}; \quad K_{II,\text{local}} = 0. \tag{30}$$

Although the stress intensity factor $K_{I,GL}$ is applied and constitutes the nominal quantity indicative of the amount of crack tip loading, an "effective" stress intensity factor $K_I = K_{I,GL} + K_{I,\text{local}}$, due to the effect of fiber bridging, actually exists at the crack tip. This depends strongly of the properties of fiber-matrix interface, as is clearly seen in Fig. 6, which shows $K_I/K_{I,GL}$ as a function of the parameter $\tilde{\lambda}$, which expresses the interface friction. For a larger value of $\tilde{\lambda}$, i.e., more fiber debonding, the effective stress intensity factor is smaller.

The two curves represent the two cases of fiber spacing considered, and it is again clear that the more widely spaced fibers show a larger effective stress intensity factor than the more closely spaced system. This agrees very nicely with the experimental observation of Botsis and Shafiq (1992) that the more closely spaced system is tougher than the more widely spaced one. Specifically, for $\tilde{\lambda} = 20$, the effective K_I for $s = 6$ μm is 21 percent of the nominal value, whereas for the more closely spaced $s = 3$ μm system, the effective K_I is only 13 percent of the nominal value. For a weaker fiber-matrix interface bond, $\tilde{\lambda} = 100$, the effective K_I for $s = 6$ μm is 59 percent of the nominal value, and, by comparison, for the more closely spaced $s = 3$ μm system, the effective K_I is smaller, i.e., 44 percent of the nominal value.

In either case, the fiber stress was below the ultimate fracture stress σ_{uf} of the glass fiber, for the entire range of $\tilde{\lambda}$'s considered; this indicates that for this example only fiber debonding and no fiber fracture would occur. Botsis and Shafiq (1992) and Botsis and Beldica (1994) considered the same geometrical configuration and the same level of applied stress but in a more widely spaced glass fiber system and a larger fiber diameter. Substituting for their fiber spacing and fiber diameter, the present model would also predict fiber stresses in the bridging zone below the ultimate fracture strength of the glass fibers, and this would again agree with their experimental results, in which no fiber fracture was observed. Hence, fiber bridging can reduce significantly the stress intensity factor and hence "toughen" the material, but this depends strongly on the fiber-matrix interface and the fiber spacing. The model presented in this paper allows quantifying this important qualitative observation.

It is conceivable that an increasing remotely applied stress σ_0 would lead to fracture of either some of the most remote from the crack tip fibers, or of the entire fiber bridging zone.

Table 1 Fracture of fiber bridges

$\tilde{\lambda}$*	$\sigma_{0f}/\sigma_0^{\dagger}$	$n_f^{\ddagger}$
10.0	8.68	0
30.0	10.79	3
40.0	12.11	6
50.0	13.16	9
60.0	14.21	13
90.0	17.63	16
100.0	18.68	17

* From Eq. (24b).
† σ_0 is the applied stress corresponding to the fracture toughness of the epoxy matrix; σ_{0f} is the applied stress that causes fracture of at least one of the fiber bridges.
‡ Number of fiber bridges left (out of initially 20).

This was found to depend strongly on the fiber-matrix interface parameter, $\tilde{\lambda}$, as shown in Table 1. In this table, the value of the applied stress, σ_{0f}, that first causes fracture of the fiber bridges is calculated for the entire range of $\tilde{\lambda}$'s considered, along with the number of fiber bridges left, n_f. The case of fiber spacing $s = 6$ μm is considered. The fiber bridging zone behind the crack tip consists of initially 20 fibers. It can be seen that for strong fiber-matrix interfaces, i.e., low values of $\tilde{\lambda}$, the entire fiber bridging zone breaks and no fiber bridges are left, i.e., $n_f = 0$. Notice that this implies some kind of unstable process since in this case of low $\tilde{\lambda}$, the maximum stress carried by a bridging zone with a smaller number of fibers is higher than the corresponding one with the load distributed on a larger number of fibers. However, for relatively weak fiber-matrix interfaces, that is high values of $\tilde{\lambda}$, only some of the most remote fibers break and as a result, a fiber bridging zone is still left. The applied stress that causes fracture of fiber bridges naturally increases with weaker fiber-matrix interfaces, i.e., higher values of $\tilde{\lambda}$.

Acknowledgment

The financial support of the Office of Naval Research, Mechanics Division, Grant N00014-91-J-1892, and the interest and encouragement of the Grant Monitor, Dr. Y. Rajapakse, are both gratefully acknowledged.

References

Beevers, C. J., Carlson, R. L., Bell, K., and Starke, E. A., 1984, "A Model for Fatigue Crack Closure," *Engineering Fracture Mechanics*, Vol. 19, pp. 93–100.

Botsis, J., and Shafiq, A. B., 1992, "Crack Growth Characteristics of an Epoxy Reinforced with Long Aligned Glass Fibers," *International Journal of Fracture*, Vol. 58, No. 1, pp. R3–R10.

Botsis, J., and Beldica, C., 1994, "Strength Characteristics and Fatigue Crack Growth in a Composite with Long Aligned Fibers," *International Journal of Fracture*, Vol. 69, pp. 27–50.

Budiansky, B., and Amazigo, J. C., 1989, "Toughening by Aligned, Frictionally Constrained Fibers," *Journal of the Mechanics and Physics of Solids*, Vol. 37, pp. 93–109.

Carlson, R. L., and Beevers, C. J., 1992, "Effects of Overloads and Mixed Modes on Closure," *Conference on Theoretical Concepts and Numerical Analysis of Fatigue* A. Blom and C. J. Beevers, eds., University of Birmingham, UK, Engineering Materials Advisory Services Ltd., Warley, UK, pp. 277–297.

Carlson, R. L., Kardomateas, G. A., and Bates, P. R., 1991, "The Effects of Overloads in Fatigue Crack Growth," *International Journal of Fatigue*, pp. 453–460.

Cox, B. N., James, M. R., Marshall, D. B., Morris, W. L., Rhodes, C. G., and Shaw, M., 1989, "Mechanics of Failure in Titanium Aluminide Composites," *Proceedings, 10th International SAMPE Conference*, Birmingham, UK, S. Benson et al., eds., Elsevier, Holland.

Hull, D., 1981, "An Introduction to Composite Materials," *Cambridge Solid State Science Series*, Cambridge University Press, Cambridge, UK.

Hutchinson, J. W., and Jensen, H. M., 1990, "Models of Fiber Debonding and Pullout in Brittle Composites with Friction," *Mechanics of Materials*, Vol. 9, pp. 139–162.

Kardomateas, G. A., and Carlson, R. L., 1995, "An Analysis of the Effects of Compressive Load Excursions on Fatigue Crack Growth in Metallic Materials," ASME JOURNAL OF APPLIED MECHANICS, Vol. 62, pp. 240–243.

Nemat-Nasser, S., and Hori, M., 1987, "Toughening by Partial or Full Bridging of Cracks in Ceramics and Fiber Reinforced Composites," *Mechanics of Materials,* Vol. 6, pp. 245–269.

Lekhnitskii, S. G., 1963, *Theory of Elasticity of an Anisotropic Elastic Body,* Holden-Day, San Francisco.

Press, W. H., Flannery, B. P., Teukolsky, S. A., and Vetterling, W. T., 1989, *Numerical Recipes,* Cambridge University Press, Cambridge, U.K.

Rosen, B. W., 1964, "Tensile Failure of Fibrous Composites," *AIAA Journal,* Vol. 2, No. 11, Nov., pp. 1985–1991.

Ruhinstein, A. A., and Xu, K., 1992, "Micromechanical Model of Crack Growth in Fiber-Reinforced Ceramics," *Journal of the Mechanics and Physics of Solids,* Vol. 40, pp. 105–125.

Russell, A. J., and Street, K. N., 1988, "A Constant ΔG Test for Measuring Mode I Interlaminar Fatigue Crack Growth Rates," *Composite Materials: Testing and Design (Eighth Conference),* ASTM STP 972, J. D. Whitcomb, ed., American Society for Testing and Materials, Philadelphia, pp. 259–277.

Sih, G. C., and Chen, E. P., 1981, *Mechanics of fracture,* Vol. 6, Martinus Nijhoff Publishers, The Hague, pp. 9–19, 87–99.

Sih, G. C., and Liebowitz, H., 1968, "*Mathematical theories of brittle fracture,*" *Fracture,* Vol. II, H. Liebowitz, ed., Academic Press, New York, pp. 67–190.

Sih, G. C., Paris, P. C., and Irwin, G. R., 1965, "On Cracks in Rectilinearly Anisotropic Bodies," *Int. J. Fract. Mech.,* Vol. 1, pp. 189–203.

Timoshenko, S. P., and Goodier, J. N., 1970, *Theory of Elasticity,* McGraw-Hill, New York, p. 136.

Zok, F., and Hom, C. L., 1990, "Large Scale Bridging in Brittle Matrix Composites," *Acta Metallurgica et Materialia,* Vol. 38, No. 10, pp. 1895–1904.